Comparison of multiobjective gradient-based methods for structural shape optimization

Matteo Giacomini, Jean-Antoine Désidéri, Régis Duvigneau

Comparison of multiobjective gradient-based methods for structural shape optimization

M. Giacomini , J.-A. Désidéri , R. Duvigneau

RESEARCH REPORT
N° 8511
March 2014
Project-Team Opale

ISSN 0249-6399 ISRN INRIA/RR--8511--FR+ENG

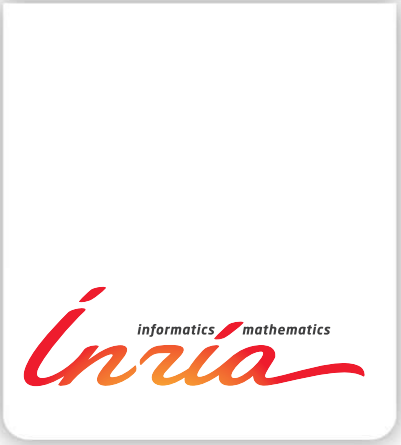

Comparison of multiobjective gradient-based methods for structural shape optimization

M. Giacomini * †, J.-A. Désidéri ‡, R. Duvigneau ‡

Project-Team Opale

Research Report n° 8511 — March 2014 — 26 pages

Abstract: This work aims at formulating a shape optimization problem within a multiobjective optimization framework and approximating it by means of the so-called *Multiple-Gradient Descent Algorithm* (*MGDA*), a gradient-based strategy that extends classical *Steepest-Descent Method* to the case of the simultaneous optimization of several criteria. We describe several variants of *MGDA* and we apply them to a shape optimization problem in linear elasticity using a numerical solver based on *IsoGeometric Analysis* (IGA). In particular, we study a multiobjective gradient-based method that approximates the gradients of the functionals by means of the Finite Difference Method; kriging-assisted *MGDA* that couples a statistical model to predict the values of the objective functionals rather than actually computing them; a variant of *MGDA* based on the analytical gradients of the functionals extracted from the *NURBS*-based parametrization of the *IGA* solver. Some numerical simulations for a test case in computational mechanics are carried on to validate the methods and a comparative analysis of the results is presented.

Key-words: Multiobjective optimization, Pareto-optimal solutions, gradient descent, IsoGeometric Analysis, shape optimization, shape gradient, kriging models

* CMAP Ecole Polytechnique, Route de Saclay, 91128 Palaiseau, France.
† Institut Polytechnique des Sciences Avancées, 7-9 rue M. Grandcoing, 94200 Ivry-sur-Seine, France.
‡ INRIA Sophia Antipolis - OPALE Team, 2004 route des Lucioles, 06902 Sophia Antipolis, France.

RESEARCH CENTRE
SOPHIA ANTIPOLIS – MÉDITERRANÉE

2004 route des Lucioles - BP 93
06902 Sophia Antipolis Cedex

Comparaison des méthodes à gradients multiples pour l'optimisation de forme en problèmes d'élasticité

Résumé : Dans ce papier on étudie un problème d'optimisation de forme en utilisant des techniques d'optimisation multiobjectif. Ce problème est abordé par la méthode à gradients multiples *MGDA* (*Multiple-Gradient Descent Algorithm*) qui est une extension de la méthode de la plus forte pente au cas de l'optimisation coopérative des plusieurs fontionnelles au même temps. On introduit trois variantes basées sur la méthode à gradients multiples et on les applique au cas d'optimisation de forme pour un problème d'élasticité linéaire approximé par l'Analyse IsoGéométrique (*IGA*). En particulier, on étudie une méthode à gradients multiples oú les gradients des fonctionnelles sont approximés par la méthode des Différences Finies; un couplage de l'algorithme *MGDA* avec un modèle de krigeage pour la prédiction statistique des valeurs des fonctionnelles; une variante de *MGDA* qui utilise les gradients analytiques des fonctionnelles extraits du solveur *IGA* grâce à la paramétrisation basée sur les fonctions de base *NURBS*. Des simulations numériques pour un cas test en mécanique sont proposées et une analyse comparative des méthodes et des résultats est présentée.

Mots-clés : Optimisation multiobjectif, solutions Pareto-optimales, descente du gradient, Analyse IsoGéométrique, optimisation de forme, gradient de forme, modèles de krigeage

1 Introduction

Many applications in engineering face the problem of designing the shape of a component in order to optimize some given properties. In the field of computational mechanics and structural engineering, this problem usually reads as the optimization of a structure to maximize its stiffness subject to a volume constraint.

In the literature several approaches to this topic have been proposed, starting from the works of G. Allaire [1] on shape optimization and F. de Gournay et al. [5] on topological optimization. More recently there has been an increasing interest towards the application of Model Order Reduction techniques and Free-Form Deformation maps to the approximation of shape optimization problems as proposed by G. Rozza et al. [18]. The present work focuses on a different approach arising from the observation that real-life applications require the analysis of different aspects at the same time. Within this framework, classical single objective optimization methods and reduced-order models experience limitations since they are not always capable of providing a complete description of the problem under analysis. For this reason we propose to formulate the shape optimization problem within a multiobjective optimization framework.

Multiobjective optimization problems have been classically tackled by means of methodologies strongly dependent on the calibration of the parameters in the model and this limited their efficacy. A totally different approach relies on the definition of the so-called *Pareto-optimal solutions*: these configurations optimize the objective functionals and generate a set of design points among which a ranking of optimality cannot be established. In this work we consider a two-phase optimization strategy as proposed by J.-A. Désidéri in [7]: first, the objective functionals are all minimized at the same time (*Cooperative phase*) then a policy to optimize one criterion without excessively worsening the others is established (*Competitive phase*). Here we focus on the first step, optimizing all the criteria at the same time; the resulting problem is tackled using *Multiple-Gradient Descent Algorithm* (*MGDA*), a gradient-based approach that extends the *Steepest Descent Method* to the case of multiobjective optimization, as introduced in [8].

The core of this work is the comparison of three variants of the multiobjective gradient-based method *MGDA*, from both an algorithmic and a numerical point of view: we present standard *MGDA* with gradients approximated by means of the Finite Difference Method; kriging-assisted *MGDA* that couples a statistical model to predict the values of the functionals; *MGDA* that uses the analytical gradients of the functionals extracted from the linear elasticity solver. For this purpose, we test the *MGDA*-based strategies on a well-known shape optimization problem in computational mechanics [19]; for the numerical approximation of the linear elasticity problem, we use *IsoGeometric Analysis* (*IGA*) [12], a Galerkin Finite Element Method where the finite-dimensional space is constructed using *Non-Uniform Rational B-Splines* (*NURBS*) as basis functions.

The paper is organized in the following way. In section 2 we present the general framework for cooperative multiobjective optimization problems; in section 3 and 4, we introduce respectively a shape optimization problem in computational mechanics and its numerical approximation using *IsoGeometric Analysis*; then we formulate the shape optimization problem within the multiobjective optimization framework in section 5 and in section 6 we present some numerical simulations of the multiobjective gradient-based methods under analysis for a test case. Eventually, section 7 summarizes the results and outlines possible further developments.

2 The multiobjective optimization framework

Let $\Omega \subset \mathbb{R}^N$ be the space of admissible design points $\mathbf{Y}$ and let us consider n objective functionals $J_i(\mathbf{Y})$, $i = 1, \dots, n$. We suppose that $\forall i = 1, \dots, n \quad J_i(\mathbf{Y}) \in \mathcal{C}^1(\Omega)$ and we consider the mul-

tiobjective optimization problem given by the simultaneous minimization of the unconstrained criteria J_i's in $\Omega \subset \mathbb{R}^N$

$$\min_{\mathbf{Y}\in\Omega} \mathbb{J}(\mathbf{Y}) \quad , \quad \mathbb{J}(\mathbf{Y}) = (J_1(\mathbf{Y}), \ldots, J_n(\mathbf{Y}))^T \tag{1}$$

In this section we recall some classical notions in MultiDisciplinary Optimization whereas for a more general introduction to the topic we refer to the book of K. Miettinen [14].

Definition 1 (*Dominance*)**.** *A design point* $\mathbf{Y}^{(0)}$ *in the parameter space* $\Omega \subset \mathbb{R}^N$ *is said to* dominate *the design point* $\mathbf{Y}^{(1)} \in \Omega$ *in efficiency if and only if*

$$J_i(\mathbf{Y}^{(0)}) \leq J_i(\mathbf{Y}^{(1)}) \quad , \quad \forall i = 1, \ldots, n$$

and for at least one criterion the inequality is strict.
Under these assumptions, we can write $\mathbf{Y}^{(0)} \succ \mathbf{Y}^{(1)}$*, otherwise it holds*

$$\mathbf{Y}^{(0)} \not\succ \mathbf{Y}^{(1)} \quad \textit{and} \quad \mathbf{Y}^{(1)} \not\succ \mathbf{Y}^{(0)}$$

and the design points are said to be non-dominated.

The notion of dominance allows to establish a sorting criterion within a population of design points with respect to the objective functionals $J_i(\mathbf{Y})$, $i = 1, \ldots, n$ and to identify the so-called *Pareto fronts*, that is, subsets of design points which are non-dominated with respect to each other (Fig. 1). The aim of multiobjective optimization procedures is to identify the *first Pareto*

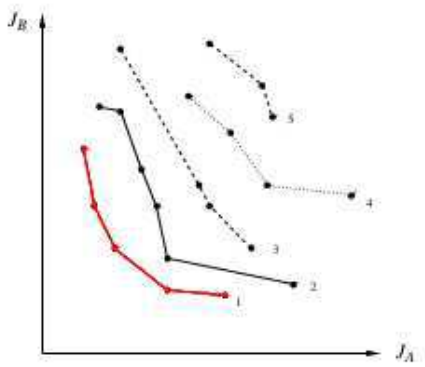

Figure 1: Pareto fronts for the multiobjective optimization of functionals J_A and J_B. In red the first Pareto front.

front, meaning the set of all design points which are Pareto-optimal.

Definition 2 (*Pareto-optimality*)**.** *Let* $\mathbf{Y}^{(0)}$ *be an admissible design point in* $\Omega \subset \mathbb{R}^N$*.* $\mathbf{Y}^{(0)}$ *is said to be* Pareto-optimal *if it is not possible to reduce the local value of any functional* $J_i(\mathbf{Y}^{(0)})$, $i = 1, \ldots, n$ *without increasing the value of at least one of the remaining criteria.*

Eventually we introduce the notion of Pareto-stationary design point as in [7]:

Definition 3 (*Pareto-stationarity*)**.** *Let* $\mathbf{Y}^{(0)}$ *be a design point at the center of an open ball within the admissible domain* $\Omega \subset \mathbb{R}^N$*. We assume that the* n *objective functionals* J_i*'s are smooth in* Ω *and we consider the local gradients* $\nabla J_i(\mathbf{Y}^{(0)})$, $i = 1, \ldots, n$*. The design point* $\mathbf{Y}^{(0)}$ *is said to be* Pareto-stationary *if and only if there exists a convex combination of the gradients that is equal to zero:*

$$\sum_{i=1}^{n} \alpha_i \nabla J_i(\mathbf{Y}^{(0)}) = 0 \quad , \quad \alpha_i \geq 0 \qquad \forall i = 1, \ldots, n \tag{2}$$

where the weights α_i*'s constitute a partition of the unity* $\sum_{i=1}^{n} \alpha_i = 1$*.*

2.1 Multiple-Gradient Descent Algorithm for cooperative optimization

Let $(\cdot, \cdot) : \mathbb{R}^N \times \mathbb{R}^N \to \mathbb{R}$ be the classical scalar product in $\mathbb{R}^N$ and $\| \cdot \| : \mathbb{R}^N \to \mathbb{R}$ the corresponding norm. We recall the main results from [8] to establish the multiobjective gradient-based strategy known as *Multiple-Gradient Descent Algorithm* proposed by J.-A. Désidéri.
First a relationship between Pareto-stationarity and Pareto-optimality is stated:

Lemma 4. *Let* $\mathbf{Y}^{(0)}$ *be an admissibile design point in* Ω*. If* $\mathbf{Y}^{(0)}$ *is Pareto-optimal, then it is Pareto-stationary.*

Thus, for the unconstrained optimization of smooth criteria, Pareto-stationarity is a necessary condition for Pareto-optimality.

Finding the descent direction common to all criteria is equivalent to finding a vector $\boldsymbol{\omega} \in \mathbb{R}^N$ such that

$$(\mathbf{u}_i, \boldsymbol{\omega}) \geq 0 \quad , \quad \mathbf{u}_i = \frac{1}{S_i} \nabla J_i(\mathbf{Y}^{(0)}) \qquad \forall i = 1, \ldots, n \tag{3}$$

where S_i , $i = 1, \ldots, n$ is a family of strictly-positive scaling factors. Thus $-\boldsymbol{\omega}$ is one descent direction for the multiobjective optimization problem (1).
Using the gradients $\mathbf{u}_i$'s as defined in (3) we can construct the following convex hull

$$\overline{\mathcal{U}} = \left\{ \mathbf{u} \in \mathbb{R}^N \quad \middle| \quad \mathbf{u} = \sum_{i=1}^{n} \alpha_i \mathbf{u}_i \quad , \quad \alpha_i \geq 0 \quad \forall i = 1, \ldots, n \quad \sum_{i=1}^{n} \alpha_i = 1 \right\} \tag{4}$$

and by exploiting its properties we can establish a general result of existence and uniqueness of a minimizing element in $\overline{\mathcal{U}}$.

Lemma 5. *Let* $\overline{\mathcal{U}}$ *be the convex hull defined in (4). There exists one realization of a minimum in* $\overline{\mathcal{U}}$ *and the minimal-norm element* $\boldsymbol{\omega}$ *is unique.*

Thanks to the characterization of $\boldsymbol{\omega}$ as the minimal-norm element in $\overline{\mathcal{U}}$, $\forall \mathbf{u} \in \overline{\mathcal{U}}$ we have that $(\mathbf{u}, \boldsymbol{\omega}) \geq \|\boldsymbol{\omega}\|^2$.

Hence a dichotomy result is established in theorem 6 stating whether a given design point is Pareto-stationary or there exists a descent direction common to all criteria.

Theorem 6. *Under the assumptions made in proposition 4, two cases are possible:*

(i) either $\boldsymbol{\omega} = \mathbf{0}$ *and the design point* $\mathbf{Y}^{(0)}$ *is Pareto-stationary;*

(ii) or $\boldsymbol{\omega} \neq \mathbf{0}$ *and in correspondance of the design point* $\mathbf{Y} = \mathbf{Y}^{(0)}$ *the vector* $-\boldsymbol{\omega}$ *defines a descent direction common to all the criteria.*

Moreover, if (ii) holds and $\boldsymbol{\omega}$ *belongs to the interior* $\mathcal{U}$ *of* $\overline{\mathcal{U}}$ *then the gradients are all equal*

$$(\mathbf{u}_i, \boldsymbol{\omega}) = \|\boldsymbol{\omega}\|^2 \qquad , \qquad \forall i = 1, \dots, n$$

and more generally for the scalar product it holds

$$(\mathbf{u}, \boldsymbol{\omega}) = \|\boldsymbol{\omega}\|^2 \qquad , \qquad \forall \mathbf{u} \in \overline{\mathcal{U}}.$$

Multiple-Gradient Descent Algorithm can either stop after a finite number of iterations achieving a Pareto-stationary design point or generate an infinite sequence of iterates. In this case, it admits a subsequence that converges to a Pareto-stationary design point. For all the details about the theoretical foundation of *MGDA*, we refer to [8].

3 Shape optimization in computational mechanics

In this section we introduce the problem of designing the optimal shape of a structure whose behaviour is governed by linear elasticity equations. We start by recalling the notion of derivation with respect to the domain. Let $\mathcal{T}$ be the space of diffeomorfism transformations in $\mathbb{R}^d$ defined as

$$\mathcal{T} = \left\{ T : \mathbb{R}^d \to \mathbb{R}^d \;\middle|\; (T - I) \in W^{1,\infty}\left(\mathbb{R}^d; \mathbb{R}^d\right) \;,\; (T^{-1} - I) \in W^{1,\infty}\left(\mathbb{R}^d; \mathbb{R}^d\right) \right\} \tag{5}$$

thus we can introduce the following space of the admissible shapes arising from a deformation of a domain D_0:

$$\mathcal{O}_{\mathcal{T}}(D_0) = \left\{ D \;\middle|\; \exists T \in \mathcal{T} \text{ such that } D = T(D_0) \right\} \tag{6}$$

Let $\mathbf{v} : \mathbb{R}^d \to \mathbb{R}^d$ be an admissible vector field that induces a sufficiently smooth deformation of the shape. A transformation $T_t : \mathbb{R}^d \to \mathbb{R}^d$ that maps an initial domain D_0 into the moving domain at time t is said to be a *perturbation of the identity* if it holds

$$D_t = T_t(\mathbf{v})(D_0) = (I + t\mathbf{v})(D_0) \quad , \quad \mathbf{v} \in W^{1,\infty}\left(\mathbb{R}^d; \mathbb{R}^d\right) \tag{7}$$

Let $\mathcal{F} : \mathcal{O}_{\mathcal{T}}(D_0) \to \mathbb{R}$ be an objective functional. Since the domain evolves during the execution of the optimization algorithm, we have to consider the way $\mathcal{F}$ changes accordingly to these variations, that is its Fréchet derivative:

$$d\mathcal{F}(D_0; \mathbf{v}) = \lim_{t \searrow 0} \frac{\mathcal{F}(D_t) - \mathcal{F}(D_0)}{t} = \langle \nabla \mathcal{F}(D_0) \;,\; \mathbf{v} \rangle_{\mathcal{D}'(\mathbb{R}^d; \mathbb{R}^d) \times \mathcal{D}(\mathbb{R}^d; \mathbb{R}^d)} \tag{8}$$

If $\forall \mathbf{v} \in \mathcal{D}(\mathbb{R}^d; \mathbb{R}^d)$ the map $\mathbf{v} \mapsto d\mathcal{F}(D_0; \mathbf{v})$ is linear and continuous, then $\mathcal{F}$ is said to be *differentiable with respect to the domain* D_0 and $\nabla \mathcal{F}(D_0)$ in equation (8) is known as the *shape gradient* of $\mathcal{F}$.

From Hadamard-Zolésio's structure theorem [9], we remark that there exists a scalar distribution $g(D_0)$ with support within ∂D_0 such that $g(D_0) \in \mathcal{D}'(\partial D_0)$ and

$$d\mathcal{F}(D_0; \mathbf{v}) = \langle g(D_0), \mathbf{v} \cdot \mathbf{n} \rangle_{\mathcal{D}'(\partial D_0) \times \mathcal{D}(\partial D_0)} \qquad \forall \mathbf{v} \in \mathcal{D}(\mathbb{R}^d, \mathbb{R}^d)$$

and if $g(D_0) \in L^1(\partial D_0)$ it holds

$$d\mathcal{F}(D_0; \mathbf{v}) = \int_{\partial D_0} g(D_0) \mathbf{v} \cdot \mathbf{n} d\sigma \tag{9}$$

3.1 Linear elasticity problem

We consider an open domain $D \subset \mathbb{R}^d$ $d = 2, 3$ which describes a deformable object subject to external forces. The boundary ∂D is composed by three disjoint parts Γ_D, Γ_N and Γ such that $\partial D = \Gamma_D \cup \Gamma_N \cup \Gamma$ and $\Gamma_D \cap \Gamma_N = \emptyset$, $\Gamma_N \cap \Gamma = \emptyset$ and $\Gamma \cap \Gamma_D = \emptyset$. A Dirichlet boundary condition representing imposed displacements is prescribed on Γ_D; on Γ_N we impose the value of the stress tensor by means of a Neumann condition whereas Γ is a free boundary whose shape has to be optimized and we prescribe homogeneous Neumann conditions on it.

We consider the static equilibrium of an isolated system by assuming zero distributed body forces. The governing equations for the problem are the classical linear elasticity equations based on the assumption of small deformations [1]:

$$\begin{cases} -div\boldsymbol{\sigma}(\mathbf{u}) = \mathbf{0} & , \quad D \\ \mathbf{u} = \mathbf{0} & , \quad \Gamma_D \\ \boldsymbol{\sigma}(\mathbf{u}) \cdot \mathbf{n} = \mathbf{g} & , \quad \Gamma_N \\ \boldsymbol{\sigma}(\mathbf{u}) \cdot \mathbf{n} = \mathbf{0} & , \quad \Gamma \end{cases} \tag{10}$$

where $\mathbf{u}$ represents the displacement field, $\boldsymbol{\sigma}(\mathbf{u})$ is the second-order Cauchy stress tensor

$$\boldsymbol{\sigma}(\mathbf{u}) = 2\mu\boldsymbol{\epsilon}(\mathbf{u}) + \lambda tr(\boldsymbol{\epsilon}(\mathbf{u}))\mathbf{I}d \tag{11}$$

μ and λ are the Lamé parameters of the material and $\boldsymbol{\epsilon}(\mathbf{u})$ is the linearized Green-Lagrange strain tensor under the assumption of small deformations

$$\boldsymbol{\epsilon}(\mathbf{u}) = \frac{1}{2}\Big(\nabla\mathbf{u} + \nabla\mathbf{u}^T + \nabla\mathbf{u}^T \cdot \nabla\mathbf{u}\Big) \approx \frac{1}{2}\Big(\nabla\mathbf{u} + \nabla\mathbf{u}^T\Big)$$

3.1.1 Variational formulation of the linear elasticity problem

In order to discretize problem (10), let us introduce the functional space

$$V = \big\{\boldsymbol{\varphi} \in (H^1(D))^d \ , \ \boldsymbol{\varphi} = \mathbf{0} \text{ on } \Gamma_D\big\}$$

The variational form of problem (10) reads as follows: we seek a displacement field $\mathbf{u} \in V$ such that

$$\int_D \left(2\mu\boldsymbol{\epsilon}(\mathbf{u}) : \boldsymbol{\epsilon}(\mathbf{v}) + \lambda div(\mathbf{u}) div(\mathbf{v})\right) d\omega = \int_{\Gamma_N} \mathbf{g} \cdot \mathbf{v} d\sigma \qquad \forall \mathbf{v} \in V \tag{12}$$

A result of existence and uniqueness of the solution for the variational linear elasticity problem may be proved within the classical framework of Lax-Milgram theorem using Korn's inequality to verify the coercivity of the bilinear form [11].

We observe that the variational formulation of the linear elasticity problem corresponds to the virtual work principles where the test function $\mathbf{v}$ in equation (12) is a virtual displacement. Thus the weak solution $\mathbf{u}$ is a minimizing configuration of the functional E

$$\min_{\mathbf{v} \in V} E(\mathbf{v}) \quad , \quad E(\mathbf{v}) = \frac{1}{2}\int_D \left(2\mu|\boldsymbol{\epsilon}(\mathbf{v})|^2 + \lambda|div(\mathbf{v})|^2\right) d\omega$$

that is, $\mathbf{u}$ realizes an equilibrium for the deformation energy E among all feasible displacement fields.

3.2 Shape optimization problem

A classical problem of shape optimization in mechanics focuses on the analysis of the configuration of the free boundary Γ which minimizes the compliance of a structure subject to a constant volume constraint.
Let us introduce the compliance $J(D)$ and the volume $G(D)$ of the structure under analysis:

$$J(D) = \int_{\Gamma_N} \mathbf{g} \cdot \mathbf{u} d\sigma \qquad , \qquad G(D) = \int_D d\omega \tag{13}$$

Therefore the shape optimization problem can be written as a constrained minimization problem in the following form:

$$\min_{D \in \mathcal{U}_{ad}} J(D) \qquad , \qquad \mathcal{U}_{ad} = \left\{ D \subset \mathbb{R}^d \ , \ G(D) = V_0 \right\} \tag{14}$$

where $\mathcal{U}_{ad}$ is the set of admissible shapes of the domain D and V_0 is the initial volume which represents the reference value for $G(D)$.

3.2.1 Existence and uniqueness of the optimal shape

We remark that all the shapes in $\mathcal{O}_{\mathcal{T}}(D_0)$ have the same topology as D_0 thus no change in the number of connected components of the boundary is possible. A general reference for the treatment of shape and topological optimization is [5].
In [1] G. Allaire proved that the map $T_t(\mathbf{v}) = I + t\mathbf{v}$ belongs to the space $\mathcal{T}$. By restricting the set of admissible shapes $\mathcal{U}_{ad}$ to small variations of the reference shape D_0 according to the following pseudo-distance in $\mathcal{O}_{\mathcal{T}}(D_0)$

$$d(D_0, D_1) = \inf_{\substack{T \in \mathcal{T} \\ T(D_0) = D_1}} \left[\|T - I\|_{W^{1,\infty}(\mathbb{R}^d, \mathbb{R}^d)} + \|T^{-1} - I\|_{W^{1,\infty}(\mathbb{R}^d, \mathbb{R}^d)} \right] \tag{15}$$

F. Murat and J. Simon [15] proved that the resulting shape optimization problem has at least one minimum point, meaning an optimal shape exists. Uniqueness of the optimal shape may only be conjectured in a general case and additional assumptions and restrictions have to be made to prove it in specific cases ([4] and [17]).

3.3 Shape derivative of the compliance

In [1] G. Allaire proved some major results about the differentiation of the compliance with respect to the domain and in particular he remarked that since the problem governed by linear elasticity equations is self-adjoint, the computation of the shape derivative of the compliance does not require the solution of an adjoint problem.
Hence under the assumptions $\mathbf{g}, \mathbf{u} \in H^2(D)$ the shape derivative of the compliance with respect to the domain D for a given shape deformation $\mathbf{v}$ is

$$dJ(D; \mathbf{v}) = - \int_\Gamma \Big(2\mu |\boldsymbol{\epsilon}(\mathbf{u})|^2 + \lambda |div(\mathbf{u})|^2 \Big) \mathbf{v} \cdot \mathbf{n} d\sigma \tag{16}$$

4 IsoGeometric Analysis for a linear elasticity problem

In this section we introduce the paradigm for the formulation of a solver based on *IsoGeometric Analysis* and we present the approximation of the linear elasticity problem (12) using *NURBS*-based Finite Element Galerkin method.
Let $\Omega_0 \subset \mathbb{R}^d$ be a parametric domain. *NURBS* basis functions are defined in Ω_0 as functions of the variable $\boldsymbol{\xi}$ and can be represented in the physical domain Ω by introducing a transformation F that maps Ω_0 to Ω (Fig. 2).

$$F : \Omega_0 \to \Omega \qquad , \qquad \mathbf{y}(\boldsymbol{\xi}) = F(\boldsymbol{\xi}) \tag{17}$$

A major advantage of the isogeometric paradigm lies in the use of a unique basis for the

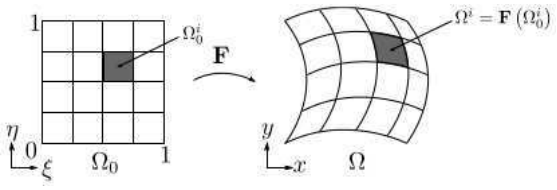

Figure 2: Transformation map F from the parametric domain Ω_0 to the physical domain Ω.

representation of the geometry of the domain and for the computational procedure: as a matter of fact, both the structural displacement field arising from the linear elasticity problem in $\mathbb{R}^d$ and the deformation field for the shape optimization algorithm in $\mathbb{R}^N$ may be written by means of *NURBS* basis functions leading to a global procedure that uses only one parametrization. Thus from now on we will indifferently refer to the computational domain by means of the space Ω of the control variables $\mathbf{Y}$ for the optimization problem.

4.1 B-Splines and Non Uniform Rational B-Splines

Let us define a *knot vector* $\Xi = (\xi_0, \ldots, \xi_a)^T \in \mathbb{R}^a$, $a = n + p + 1$, that is a vector of non-decreasing real numbers which describes the general geometrical structure of the curve. Using this notation, p is the polynomial *order* of the basis functions and n is the number of considered functions. Equally-spaced knots in the domain Ω_0 are said to be *uniform*. On the contrary we name *non-uniform* the knots that are unequally-spaced in the domain. Knots located at the same coordinates in the parametric space are known as *repeated* knots. A knot vector is said to be *open* if its first and last knots are repeated $p+1$ times. Open knot vectors are tipically used in *CAD* applications because basis functions are interpolatory at the ends of the parametric space interval.

We introduce B-Spline starting from the piecewise constant basis function ($p = 0$)

$$N_{i,0}(\xi) = \begin{cases} 1 \ , & \xi_i \leq \xi < \xi_{i+1} \\ 0 \ , & \text{otherwise} \end{cases} \tag{18}$$

and then we recursively define them for the order p as

$$N_{i,p}(\xi) = \frac{\xi - \xi_i}{\xi_{i+p} - \xi_i} N_{i,p-1}(\xi) + \frac{\xi_{i+p+1} - \xi}{\xi_{i+p+1} - \xi_{i+1}} N_{i+1,p-1}(\xi) \tag{19}$$

where the quotient $0/0$ is assumed to be zero.
In general, basis functions of order p have $p-1$ continuous derivatives and if a knot is repeated

k times, the regularity of the function drops to $\mathcal{C}^{p-k}$ in correspondance of that specific knot. When the multiplicity of a knot is exactly p the basis function is interpolatory.

Considering the set $\mathcal{I} = \{0, \ldots, n\}$, one-dimensional *Non-Uniform Rational B-splines* of degree p are given by

$$R_{k,p}(\xi) = \frac{w_k N_{k,p}(\xi)}{\sum_{i \in \mathcal{I}} w_i N_{i,p}(\xi)} \tag{20}$$

where $w_i \in \mathbb{R}$ is the weight associated to the i-th B-spline function.
Two- (respectively three-) dimensional *NURBS* basis functions are defined as the bivariate (respectively trivariate) tensor products of the one-dimensional basis functions in (20). Here we introduce two sets $\mathcal{I} = \{0, \ldots, n\}$ and $\mathcal{J} = \{0, \ldots, m\}$, two B-spline basis functions N and M and we define two knots vectors $\Xi_\xi = (\xi_0, \ldots, \xi_a)^T$ and $\Xi_\eta = (\eta_0, \ldots, \eta_b)^T$ where $a = n + p + 1$ and $b = m + q + 1$; thus the rational surfaces of degrees p and q can be expressed as

$$R_{kl,pq}(\xi, \eta) = \frac{w_{kl} N_{k,p}(\xi) M_{l,q}(\eta)}{\sum_{i \in \mathcal{I}} \sum_{j \in \mathcal{J}} w_{ij} N_{i,p}(\xi) M_{j,q}(\eta)} \tag{21}$$

and the extension to three-dimensional basis functions is straightforward.

Starting from the general form of the transformation (17), we provide some additional details for the two-dimensional case: let Ω_0 be the square $(0,1) \times (0,1)$, any point $\mathbf{y} = (x, y)^T$ in the physical domain Ω is mapped back to a point $\boldsymbol{\xi} = (\xi, \eta)^T$ in the parametric domain as described in figure 2. Thus by associating a control point to each basis function we can explicitly describe the relationship in equation (17) as

$$\mathbf{y}(\xi, \eta) = \sum_{i \in \mathcal{I}} \sum_{j \in \mathcal{J}} R_{ij}(\xi, \eta) \mathbf{Y}_{ij} \tag{22}$$

where $\mathbf{Y}_{ij} \in \mathbb{R}^2$ are the coordinates of the control point of indices (i, j) in the parametric domain.

4.2 NURBS-based Galerkin formulation

Classical numerical methods for the approximation of problem (12) first rely on the construction of a discrete domain Ω_h which is a polygonal approximation of the continuous object under analysis. Major drawbacks of this approach consist in the high computational cost required by the mesh generation process and in the numerical errors introduced by the geometrical approximation. To avoid these problems, T.J.R. Hughes et al. [12] proposed a new approach to better integrate *Finite Element Analysis* and *Computer Aided Design* by means of a unique representation suitable for both the geometry and the discrete solution: *Non-Uniform Rational B-Splines* are a *de facto* standard for geometrical modelling in *CAD* thus main idea of *IsoGeometric Analysis* consists of employing this parametric representation both for exactly describing the computational domain and for solving the governing equations without previously approximating the domain by means of a piecewise linear grid.

For the sake of simplicity, let us restrict to the two-dimensional case and let us introduce a family of *NURBS* basis functions $\widehat{R}_{ij}$'s defined in the physical domain such that

$$\widehat{R}_{ij}(\mathbf{y}) = \widehat{R}_{ij}(x, y) = \widehat{R}_{ij} \circ F(\xi, \eta) = R_{ij}(\boldsymbol{\xi}) \tag{23}$$

Thus the discretized unknown displacement field $\mathbf{u}_h(\mathbf{y})$ is constructed as convex combination of the *NURBS* functions that describe the geometry

$$\mathbf{u}_h(\mathbf{y}) = \sum_{i \in \mathcal{I}} \sum_{j \in \mathcal{J}} R_{ij}(\boldsymbol{\xi}) \mathbf{U}_{ij} = \sum_{i \in \mathcal{I}} \sum_{j \in \mathcal{J}} \widehat{R}_{ij}(\mathbf{y}) \mathbf{U}_{ij} \tag{24}$$

By considering open knot vectors, we are able to force *NURBS* functions to be interpolatory on the boundary. Thanks to this property, we can easily impose zero Dirichlet boundary conditions on Γ_D by setting to zero the coefficients $\mathbf{U}_{ij}$ that belong to the corresponding knots on Γ_D. Moreover, considering the boundary conditions as a constraint over the Degrees Of Freedom of the problem, we may rewrite the unknown field $\mathbf{u}_h$ after neglecting the basis functions that are required to enforce the zero Dirichlet boundary conditions; renumbering the remaining basis functions and unknowns with an index ℓ spanning from 1 to L, equation (24) reads as

$$\mathbf{u}_h(\mathbf{y}) = \sum_{\ell=1}^{L} \mathbf{N}_\ell(\mathbf{y}) U_\ell = \mathbf{N}(\mathbf{y})\mathbf{U} \tag{25}$$

where $\mathbf{U} \in \mathbb{R}^L$ contains the unknown displacement coefficients $\mathbf{U}_{ij}$'s corresponding to the unconstrained control points, meaning the ones where we do not impose Dirichlet boundary conditions. Moreover, each column $\mathbf{N}_\ell(\mathbf{y})$ of the $2\times L$ matrix $\mathbf{N}(\mathbf{y})$ contains the *NURBS* basis function $R_{ij}(\boldsymbol{\xi})$ split into its components along the x- and y- directions.

Hence the numerical approximation of the linear elasticity problem (10) by means of *IsoGeometric Analysis* reads as equation (12) where we substitute the continuous function $\mathbf{u}$ by its discrete counterpart $\mathbf{u}_h \in V_h$, being the finite-dimensional subspace $V_h \subset V$ given by the following span of *NURBS* basis functions

$$V_h = \langle \mathbf{N}_1, \dots, \mathbf{N}_L \rangle \tag{26}$$

4.2.1 Imposition of the boundary conditions

A critical aspect in *IsoGeometric Analysis* is represented by the correct imposition of the boundary conditions. From a modelling point of view, Dirichlet conditions correspond to setting the displacements on the boundary, meaning applying them to the corresponding control variables: this results in exact pointwise satisfaction when dealing with homogeneous conditions; otherwise the boundary data have to be properly approximated by means of functions lying in the *NURBS* space, thus introducing additional numerical errors. On the other hand, Neumann conditions have the physical meaning of imposing stresses on the boundary of the structure under analysis and are naturally satisfied by performing the integration over the boundary of the domain in the same way as in classical Finite Element formulations.

4.2.2 Discrete algebraic problem

Using the space V_h defined in (26) we can construct a stiffness matrix $K \in \mathbb{R}^{L\times L}$ and a force vector $\widetilde{\mathbf{F}} \in \mathbb{R}^L$. The algebraic formulation of the elasticity problem is straightforward:

$$K\mathbf{U} = \widetilde{\mathbf{F}} \tag{27}$$

and the components of the stiffness matrix and the force vector in equation (28) are computed using classical quadrature rules with Gaussian points in the parametric domain.

$$K_{ij} = \int_\Omega (2\mu\boldsymbol{\epsilon}(\mathbf{N}_i) : \boldsymbol{\epsilon}(\mathbf{N}_j) + \lambda div(\mathbf{N}_i) div(\mathbf{N}_j)) d\omega \qquad , \qquad \widetilde{F}_\ell = \int_{\Gamma_N} \mathbf{g}\cdot\mathbf{N}_\ell d\sigma \tag{28}$$

Since the support of the *NURBS* basis functions is larger than the one of Lagrangian basis functions, the pattern of *IGA*-based stiffness matrix is generally less sparse than the one arising from Lagrangian Finite Element Method. Nevertheless, the number of Degrees of Freedom in *IsoGeometric Analysis* is extremely lower than the one required by Lagrangian discretizations.

Algorithm	Computation of J	Computation of ∇J	Variables	Applies to
MGDA using FD	Exact through *IGA* solver	Approximated by FD on fine surrogate mesh	Control points on the coarse grid (Low number)	Single design point
Kriging-assisted *MGDA*	Predicted using kriging model	Approximated by FD on fine surrogate mesh	Control points on the coarse grid (Low number)	Set of design points
MGDA using analytical gradients	Exact through IGA solver	Extracted from *NURBS* parametrization in *IGA* solver	Control points after k-refinement (High number)	Single design point

Table 1: Settings of *MGDA*-based strategies for shape optimization using *IGA*.

This results in a lower dimension of the algebraic system (27) thus in an impressive reduction of the computational cost of the implemented solver. For the solution of linear system (27), several strategies are available. Since K is a symmetric positive definite matrix and - as previously stated - the dimension of the problem remains moderate, we choose a classical sparse direct solver such as the multi-frontal method implemented in the *UMFPACK Library*.

5 A multiobjective optimization approach to shape optimization

In this section we reformulate the structural shape optimization problem introduced in section 3.2 within the multiobjective optimization framework described in section 2 and we approximate it by means of *Multiple-Gradient Descent Algorithm*.

First, we identify a set of at least two antagonistic criteria to be the objective functionals of the cooperative multiobjective optimization problem. From equation (16) we notice that $dJ(\Omega;\mathbf{v}) < 0$ if $\mathbf{v}\cdot\mathbf{n} > 0$, that is, the compliance may always be decreased by enlarging the domain. Thus the multiobjective shape optimization problem reads as

$$\min_{\Omega\subset\mathbb{R}^d} \mathbb{J}(\Omega) \qquad , \qquad \mathbb{J}(\Omega) = \left(J(\Omega), G(\Omega)\right)^T \tag{29}$$

where $J(\Omega)$ and $G(\Omega)$ are defined as in equation (13).

In order to identify the first Pareto front as a result of the cooperative optimization procedure, we propose several variants of *MGDA*. From a practical point of view, we aim at finding a descent direction common to all the criteria such that at every iteration of the algorithm both the objective functionals decrease.
Critical aspects are represented by the high number of evaluations of the functionals and by the technique for the numerical approximation of the gradients. Table 1 summarizes the strategies investigated: on the one hand, we compare the methods to compute the objective functionals and their gradients; on the other hand, we analyze the dimension of the spaces of the optimization variables in order to quantify the computational cost of the implemented variants of *MGDA*.

5.1 Multiple-Gradient Descent Algorithm (MGDA)

Multiobjective gradient-based method *MGDA* can be seen as an extension of classical single objective *Steepest Descent Method* to the case of multiobjective optimization.

Starting from theorem 6, we outline the following procedure. First, we evaluate the n objective functionals J_i's and we compute the corresponding gradients $\mathbf{u}_i$'s. Then we determine the descent direction $-\boldsymbol{\omega}$ as the minimal-norm element in the convex hull $\overline{\mathcal{U}}$ (see section 5.1.1). Eventually, we perform a line search to identify the optimal step size $\widetilde{\rho}$ that guarantees the best improvement of the objective functionals during the transition from $J_i(\mathbf{Y})$ to $J_i(\mathbf{Y} - \widetilde{\rho}\boldsymbol{\omega})$ $\forall i = 1, \dots, n$ (see section 5.1.2).

5.1.1 Computing the descent direction

We recall that every element in the convex hull $\overline{\mathcal{U}}$ may be written as a convex combination of the scaled gradients $\mathbf{u}_i$, $i = 1, \dots, n$. Thus the problem of computing the descent direction reads as the constrained minimization of the quadratic form that expresses $\|\boldsymbol{\omega}\|^2$ in terms of the coefficients $\boldsymbol{\alpha} = (\alpha_1, \dots, \alpha_n)^T$ of the convex combination:

$$\min_{\boldsymbol{\alpha} \in A_{ad}} \left\| \sum_{i=1}^{n} \alpha_i \mathbf{u}_i \right\|^2 \tag{30}$$

where $A_{ad} \subset \mathbb{R}^n$ is the set of the admissible vectors $\boldsymbol{\alpha}$ such that their components are non-negative and they constitute a partition of the unity:

$$A_{ad} = \left\{ \boldsymbol{\alpha} \in \mathbb{R}^n \quad \middle| \quad \alpha_i \geq 0 \quad \forall i = 1, \dots, n \quad , \quad \sum_{i=1}^{n} \alpha_i = 1 \right\} \tag{31}$$

For the case of two objective functionals as the shape optimization problem in equation (29), the minimal-norm element is given by $\boldsymbol{\omega} = \gamma \mathbf{u}_1 + (1-\gamma)\mathbf{u}_2$ where the coefficients $\alpha_1 = \gamma$ and $\alpha_2 = 1 - \gamma$ of the convex combination can be explicitly expressed in a closed form. Let us construct the quadratic function

$$\ell(\gamma) = \|\gamma \mathbf{u}_1 + (1-\gamma)\mathbf{u}_2\|^2 = (\gamma \mathbf{u}_1 + (1-\gamma)\mathbf{u}_2, \gamma \mathbf{u}_1 + (1-\gamma)\mathbf{u}_2) \tag{32}$$

Beyond the trivial case where $\mathbf{u}_1 = \mathbf{u}_2$, for the first-order optimality condition $\ell'(\gamma) = 0$, the minimum is achieved for

$$\gamma = -\frac{\mathbf{u}_2 \cdot (\mathbf{u}_1 - \mathbf{u}_2)}{\|\mathbf{u}_1 - \mathbf{u}_2\|^2} = \frac{\|\mathbf{u}_2\|^2 - \mathbf{u}_2 \cdot \mathbf{u}_1}{\|\mathbf{u}_1\|^2 + \|\mathbf{u}_2\|^2 - 2\mathbf{u}_1 \cdot \mathbf{u}_2} \tag{33}$$

In [8] the author analyzed the admissible values for the angle $\theta = \widehat{(\mathbf{u}_1, \mathbf{u}_2)}$ and identified a condition to guarantee that $\gamma \in (0, 1)$ in a general case by requiring the angle θ to be obtuse, that is $\mathbf{u}_1 \cdot \mathbf{u}_2 < 0$.
Hence for the two-dimensional case, the coefficient γ assumes the following expression:

$$\gamma = \begin{cases} 0 & , \quad \min\{\|\mathbf{u}_1\|, \|\mathbf{u}_2\|\} = \|\mathbf{u}_2\| \\ -\dfrac{\mathbf{u}_2 \cdot (\mathbf{u}_2 - \mathbf{u}_1)}{\|\mathbf{u}_1 - \mathbf{u}_2\|^2} & , \quad \mathbf{u}_1 \cdot \mathbf{u}_2 < \Big(\min\{\|\mathbf{u}_1\|, \|\mathbf{u}_2\|\} \Big)^2 \\ 1 & , \quad \min\{\|\mathbf{u}_1\|, \|\mathbf{u}_2\|\} = \|\mathbf{u}_1\| \end{cases} \tag{34}$$

5.1.2 Line search for the optimal step size

Computing a step that improves all the criteria and gives significant evolution to the problem is not a trivial task. In general, an adaptive method to compute the best step at every iteration

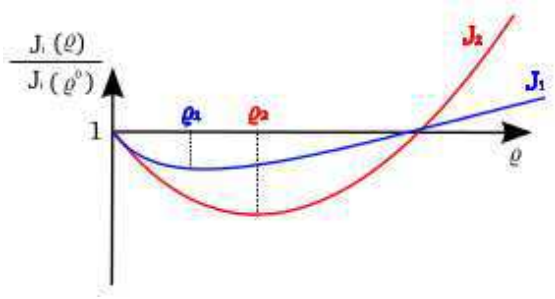

Figure 3: Line search for the optimal step size ρ along the descent direction $-\boldsymbol{\omega}$.

would be convenient.
We proceed by defining $\forall i = 1, \ldots, n$ the functions $j_i : \mathbb{R} \to \mathbb{R}$ such that $j_i(\rho) = J_i(\mathbf{Y} - \rho\boldsymbol{\omega})$. Basic idea is to identify the optimal step size $\widetilde{\rho}$ such that $\widetilde{\rho}$ is the largest strictly positive real number for which every $j_i(\widetilde{\rho})$, $i = 1, \ldots, n$ is monotone descreasing on the interval $[0, \widetilde{\rho}]$.
For this purpose a surrogate quadratic model is constructed and a bisection strategy to identify the zero of $j_i'(\rho)$ is performed $\forall i = 1, \ldots, n$. The optimal step size $\widehat{\rho}_i$ for the function $j_i(\rho)$ is a minimum for the surrogate model and the smallest among the $\widehat{\rho}_i$'s is chosen to be the optimal step $\widetilde{\rho}$ for the global procedure as illustrated in figure 3:

$$\widetilde{\rho} = \min_{1 \leq i \leq n} \widehat{\rho}_i$$

5.1.3 Shape optimization procedure using *MGDA*

Concerning the linear elasticity problem in equation (10), the boundary is parametrized by means of *Non-Uniform Rational B-Splines* thus the design point that describes the configuration of the system is the vector of the control points of the *NURBS* curve Γ.
The routine listed in script 1 describes the evolution of a single design point towards a Pareto-stationary configuration and it has to be performed for an adequate set of design points in order to obtain a good description of the Pareto front.

Listing 1: Shape optimization procedure using *MGDA* with Finite Differences

```
1. Generate the initial geometry;
2. Run the IGA solver to compute the compliance and the volume;
3. Generate a surrogate FD mesh to compute the gradients of the functionals;
4. Identify the descent direction −ω as convex combination of ∇J(Y) and ∇G(Y);
5. Determine the optimal step size ρ̃ by means of a bisection algorithm;
6. Update the design vector Y to Y − ρ̃ω;
7. If ‖ω‖ ≥ tol, go to step 1; otherwise a Pareto-stationary design point has been
   achieved and the optimization procedure is stopped.
```

First, the algorithm evaluates the objective functionals $J(\mathbf{Y})$ and $G(\mathbf{Y})$ invoking the *IsoGeometric Analysis* solver once. Then the optimization loop begins: a surrogate conforming grid is constructed using a very fine step size and the gradients of the functionals are computed by means of a second order centered Finite Difference scheme. We remark that to perform this operation the values of the functionals $J(\mathbf{Y})$ and $G(\mathbf{Y})$ have to be computed in correspondance of two adjacent spatial nodes, thus the *IGA* solver has to be invoked $2q$ times where q is the global number of the control points used to describe Γ.

The descent direction $-\boldsymbol{\omega}$ and the optimal step size $\widetilde{\rho}$ that guarantee the cooperative minimization of both criteria are identified and the design point is updated. The iterative loop ends when the point under analysis is Pareto-stationary, that is when $\|\boldsymbol{\omega}\|$ is smaller than an *a priori* fixed tolerance.

A satisfactory description of the Pareto front requires 20 to 40 design points, each of which is obtained after 30 to 50 iterations of *MGDA*. Since for every run of the optimization algorithm, the solver is invoked $2q+1$ times to evaluate the functionals and compute the components of the gradients, the resulting computational cost of this strategy is very demanding.

5.2 Metamodel-assisted MGDA optimization

In order to reduce the computational cost associated with the numerical solution of the physical problem under analysis for a large number of configurations, in [20] A. Zerbinati et al. proposed to couple *MGDA* with a statistical model to predict the objective functionals rather than actually computing them. Basic idea of the global optimization procedure is reported in figure 4.

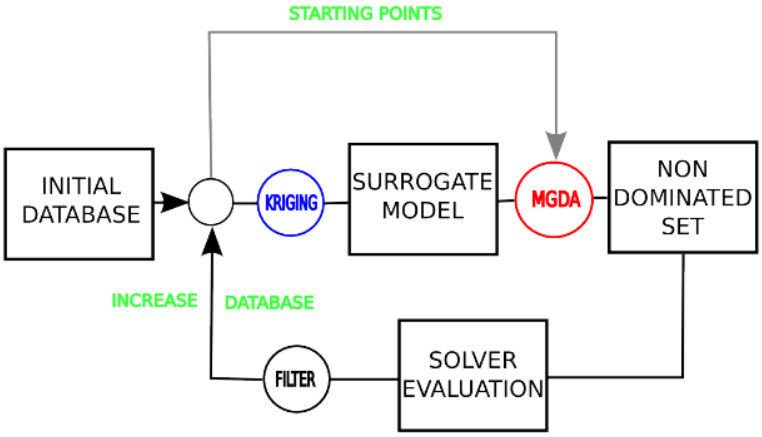

Figure 4: Global procedure for kriging-assisted *MGDA* optimization.

5.2.1 Kriging-based metamodel

The statistical approach proposed in [6] and used in this work is based on a technique to predict spatial data, namely kriging models. Let us introduce for each objective functional J_i, a novel functional $j_k = J_i(\mathbf{Y}^{(k)})$, $\mathbf{Y}^{(k)} \in \Omega$. Kriging models rely on the assumption that the values $J_N = \{j_1, \dots, j_N\}$ computed in correspondance of a set of design points $\left\{\mathbf{Y}^{(1)}, \dots, \mathbf{Y}^{(N)}\right\}$ are one realization of a multivariate Gaussian stochastic process with joint probability density

$$\mathbb{P}(J_N) = \frac{1}{\sqrt{(2\pi)^N |\Sigma_N|}} exp\left\{-\frac{1}{2} J_N^T \Sigma_N^{-1} J_N\right\} \tag{35}$$

where Σ_N is the $N \times N$ covariance matrix that expresses the correlation among the realizations associated with different design points. Moreover we suppose that the value J_{N+1} of the objective functional obtained when adding a new design point $\mathbf{Y}^{(N+1)}$ to the model is itself a realization of a $(N+1)$-dimensional Gaussian process whose covariance matrix Σ_{N+1} may be factorized in

the following blocks

$$\Sigma_{N+1} = \begin{bmatrix} \Sigma_N & \mathbf{k} \\ \mathbf{k}^T & \kappa \end{bmatrix}$$

where $\mathbf{k}$ and κ represent respectively the covariance among the new design point $\mathbf{Y}^{(N+1)}$ and the previous existing ones and its variance:

$$\mathbf{k} = [\sigma(\mathbf{Y}^{(1)}, \mathbf{Y}^{(N+1)}), \dots, \sigma(\mathbf{Y}^{(N)}, \mathbf{Y}^{(N+1)})] \quad , \quad \kappa = \sigma(\mathbf{Y}^{(N+1)}, \mathbf{Y}^{(N+1)}) \tag{36}$$

Thus for the conditional probability density of the unknown functional value j_{N+1} given the data J_N we have

$$\mathbb{P}(j_{N+1} \mid J_N) \propto exp\left\{ -\frac{(j_{N+1} - \widehat{j}_{N+1})^2}{2\sigma^2_{N+1}} \right\} \tag{37}$$

where its mean $\widehat{j}_{N+1}$ is the prediction of the kriging model at the new point $\mathbf{Y}^{(N+1)}$:

$$\widehat{j}_{N+1} = \mathbf{k}^T \Sigma_N^{-1} J_N \qquad , \qquad \sigma^2_{N+1} = \kappa - \mathbf{k}^T \Sigma_N^{-1} \mathbf{k}$$

The application of a statistical-based prediction introduces an additional error in the approximation of the problem but the evaluation of the variance σ^2_{N+1} allows to monitor the uncertainty due to the kriging model and to control it. More details on this topic are available in [6].

5.2.2 Shape optimization procedure using kriging-assisted *MGDA*

As for *MGDA* procedure in section 5.1.3, we consider the control points of the free boundary Γ as optimization variables.
During an initial phase, a data set of design points is generated using *Latin Hypercube Sampling* to uniformly map the whole domain of computation (Script 2). For each configuration, the *IGA* solver is invoked and the corresponding values of the objective functionals are computed. These entries will be later used both for the prediction of the values of the functionals by means of the kriging model and as starting point for the computation of *MGDA* iterates.

Listing 2: Shape optimization procedure using kriging-assisted *MGDA* - Construction of the initial data set

```
1. Build an initial data set using Latin Hypercube Sampling in ℝ^{2q} where 2q is the
   number of components of the design vector;
2. For each entry of the data set generate an initial geometry;
3. Run the IGA solver to compute the compliance and the volume;
4. Store the values of the functionals in the data set.
```

A critical step in the construction of the initial data set is represented by the compatibility that has to be enforced between the physical problem and its discrete numerical representation since initial control points are randomly generated. In particular, repeated control points or control points very close to one another may generate issues in the control polygon leading to kinks and singularities to appear in the representation of curves and surfaces within the isogeometric paradigm. Hence inaccurate initial control points may cause non-physical scenarios to arise in the analysis of stresses and displacements in a linear elasticity problem.

In script 3 we present the global optimization procedure starting from the previously defined data set. First, we refer to the construction of the kriging model presented by R. Duvigneau et al. in [6]: a function that describes the dependency among the data has to be determined by

estimating the spatial correlation with respect to a particular stochastic process. This results in the minimization of the log-likelihood function

$$\mathcal{L} = J_N^T \Sigma_N^{-1} J_N + \log |\Sigma_N|$$

by means of a *Particle Swarm Optimization* technique that is robust and not sensitive to local minima since $\mathcal{L}$ is a multi-modal function. The parameters of this model are tuned by minimizing the mean square error under the constraint of unbiasedness. The values of the objective functionals corresponding to a point that lies in the region where the improvement of the criteria is expected to be the most significant are iteratively constructed from the linear combination of previously known ones.

Then each entry of the data set is used as starting point to run *Multiple-Gradient Descent Algorithm* until a Pareto-stationary point is achieved; the computation of the gradients of the functionals is still performed by means of a second order centered Finite Difference scheme on a surrogate conforming grid. However, the *IGA* solver is invoked only when a Pareto-stationary design point is achieved whereas the intermediate steps are handled by means of the previously discussed kriging prediction.

Final *MGDA* points are directly evaluated using the numerical solver of the problem and the resulting information is added to the existing data set to enrich the precision of the statistical model. In order to mantain the dimension of the problem as small as possible, a filter is applied and new design points are discarded if too close to already existing entries. At completion of the enrichment process, the metamodel is updated and training is performed again in order to refine the information carried by the surrogate model and consequently better predict the objective functionals corresponding to the new design points.

Listing 3: Shape optimization procedure using kriging-assisted *MGDA* - Metamodel-assisted optimization

1. Perform the training of the data set and calibrate the parameters that describe the correlation among the data;
2. Perform kriging prediction of the functional values;
3. Generate a surrogate FD grid to compute the gradients of the functionals using kriging estimations;
4. Identify the descent direction $-\boldsymbol{\omega}$ as convex combination of $\nabla J(\mathbf{Y})$ and $\nabla G(\mathbf{Y})$;
5. Determine the optimal step size $\widetilde{\rho}$ by means of a bisection algorithm;
6. Update the design vector $\mathbf{Y}$ to $\mathbf{Y} - \widetilde{\rho}\boldsymbol{\omega}$;
7. If $\|\boldsymbol{\omega}\| \geq tol$, go to step 2; otherwise a Pareto-stationary design point has been achieved;
8. Generate the corresponding geometry and run the IGA solver to compute the compliance and the volume for final MGDA points and enrich the data set;
9. Filter the data set to eliminate non-informative configurations;
10. If the number of iterates is not over, go to step 1; otherwise, stop the algorithm: a set of Pareto-stationary solutions has been identified.

The resulting configurations are non-dominated design points, thus they belong to the first Pareto front associated with the optimization problem under analysis. We remark that the kriging-assisted optimization strategy is performed an *a priori* fixed number of times that has to be properly calibrated in order to obtain a robust method.

From a computational point of view, main advantage of kriging-assisted *MGDA* is the reduction of the computational effort. As a matter of fact, the method applies to a set of design points at the same time and invokes the *IGA* solver only to evaluate last *MGDA* iterate. This results in the parallel evolution of several design points, leading to a complete description of the Pareto front in 10 to 15 runs of the global optimization strategy. Moreover, the iterative enrichment of the data set and its filtering are responsible for the improvement of the information at every iteration. Hence this procedure may be considered a *predictor-corrector* optimization strategy.

5.3 MGDA using analytical gradients

The isogeometric paradigm allows to conveniently express the domain boundaries in terms of control points and *NURBS* basis functions. We recall the form of the transformation (17) which maps the parametric domain Ω_0 into the physical one Ω:

$$\mathbf{y}(\boldsymbol{\xi}) = \mathbf{y}(\xi,\eta) = \sum_{i\in\mathcal{I}}\sum_{j\in\mathcal{J}} R_{ij}(\xi,\eta)\mathbf{Y}_{ij}$$

where $\mathbf{Y}_{ij} = (X_{ij}, Y_{ij})$ and $\mathbf{y}_{ij} = (x_{ij}, y_{ij})$ are respectively the control points in the parametric and physical domain.
Thus the Jacobian matrix arising from the transformation (17) is given by

$$\mathrm{J} = \begin{bmatrix} \sum_{i,j} R_{ij,\xi} X_{ij} & \sum_{i,j} R_{ij,\xi} Y_{ij} \\ \sum_{i,j} R_{ij,\eta} X_{ij} & \sum_{i,j} R_{ij,\eta} Y_{ij} \end{bmatrix} \tag{38}$$

where $i \in \mathcal{I},\ \ j \in \mathcal{J}$ and the *NURBS* basis functions are $R_{ij} = R_{ij}(\xi,\eta)$.
Thanks to the use of *NURBS*-based parametrization, we are able to extract the information on the gradients ∇G and ∇J with respect to the control points $\mathbf{Y}_{kl}$ in the parametric space directly from the *IGA* solver.

5.3.1 Gradient of the volume in the parametric space

The volume functional $G(\mathbf{Y})$ only depends on the geometrical information of the domain. We map Ω back to Ω_0 and we integrate over the parametric domain using Gaussian quadrature points.

$$\begin{aligned} G(\mathbf{Y}) &= \int_\Omega d\omega = \iint_{\xi,\eta} |\mathrm{J}| d\xi d\eta = \\ &= \iint_{\xi,\eta} \Big(\sum_{i,j} R_{ij,\xi} X_{ij} \cdot \sum_{i,j} R_{ij,\eta} Y_{ij} - \sum_{i,j} R_{ij,\xi} Y_{ij} \cdot \sum_{i,j} R_{ij,\eta} X_{ij} \Big) d\xi d\eta \end{aligned} \tag{39}$$

Thanks to the linearity of the operator $\mathbf{Y} \mapsto G(\mathbf{Y})$ it is straightforward to differentiate (39) with respect to the control variables $\mathbf{Y}_{kl}$'s thus the components of ∇G read as

$$\begin{aligned} \frac{\partial}{\partial X_{kl}} G &= \iint_{\xi,\eta} \Big(R_{kl,\xi} \sum_{i,j} R_{ij,\eta} Y_{ij} - R_{kl,\eta} \sum_{i,j} R_{ij,\xi} Y_{ij} \Big) d\xi d\eta \\ \frac{\partial}{\partial Y_{kl}} G &= \iint_{\xi,\eta} \Big(R_{kl,\eta} \sum_{i,j} R_{ij,\xi} X_{ij} - R_{kl,\xi} \sum_{i,j} R_{ij,\eta} X_{ij} \Big) d\xi d\eta \end{aligned} \tag{40}$$

5.3.2 Gradient of the compliance in the parametric space

The computation of the gradient of the compliance with respect to the control points $\mathbf{Y}_{kl}$'s relies on the ability to express the shape derivative $dJ(\Omega;\mathbf{v})$ as in equation (9).
We recall the general form of the shape derivative of the compliance (16):

$$dJ(\Omega;\mathbf{v}) = \int_\Gamma B\mathbf{v}\cdot\mathbf{n} d\sigma \qquad , \qquad B = -\Big(2\mu|\boldsymbol{\epsilon}(\mathbf{u})|^2 + \lambda|div(\mathbf{u})|^2 \Big) \tag{41}$$

Starting from the works of J.-P. Zolésio [9] and J. Cea [3], we express the domain Ω as a *NURBS* surface. The admissible deformation $\mathbf{v}$ applied to Ω is a *NURBS* surface itself

$$\mathbf{v} = \sum_{k\in\mathcal{I}}\sum_{l\in\mathcal{J}} R_{kl}(\xi,\eta)\mathbf{V}_{kl} = \sum_{k\in\mathcal{I}}\sum_{l\in\mathcal{J}} R_{kl}(\xi,\eta)\left(V_{kl}^{(1)}\ ,\ V_{kl}^{(2)}\right)^T$$

and the normal direction to the *NURBS* surface is identified by the two-dimensional cross product between the partial derivatives of $\mathbf{y}$ with respect to ξ and η

$$\mathbf{n} = \frac{1}{|\mathrm{J}|}\sum_{i\in\mathcal{I}}\sum_{j\in\mathcal{J}} R_{ij,\xi}(\xi,\eta)\,(Y_{ij}\ ,\ -X_{ij})^T$$

Moreover, the boundary Γ can also be expressed as a *NURBS* curve thus by combining all the previous results, the shape derivative of the compliance reads as

$$dJ(\Omega;\mathbf{v}) = \sum_{k,l}\sum_{i,j} a_{ij}^{kl}\,(Y_{ij}\ ,-X_{ij}\ )\left(V_{kl}^{(1)}\ ,\ V_{kl}^{(2)}\right)^T \quad , \quad a_{ij}^{kl} = \iint_{\xi,\eta} BR_{kl}R_{ij,\xi}d\xi d\eta \tag{42}$$

where the indices i,k and j,l span respectively over the sets $\mathcal{I}$ and $\mathcal{J}$. For the sake of readibility, the dependency of the basis functions R_{kl} and their derivatives $R_{ij,\xi}$ on the parametric variables (ξ,η) is omitted.
Hence from equation (42) it is straightforward to isolate the components of the gradient of the compliance with respect to the control points:

$$\frac{\partial}{\partial X_{kl}}J = \sum_{i,j} a_{ij}^{kl}Y_{ij} \qquad , \qquad \frac{\partial}{\partial Y_{kl}}J = -\sum_{i,j} a_{ij}^{kl}X_{ij} \tag{43}$$

5.3.3 Shape optimization procedure using *MGDA* with analytical gradients

We start from the framework introduced in 5.1.3 and we replace the numerical computation of the gradients by the extraction of the same information from the *IGA* solver: the computation of the gradients by means of Finite Difference routines is avoided and the expression of the partial derivatives of the objective functionals with respect to the control points are given by equations (40) and (43).

We remark that during the execution of the isogeometric solver an enrichement of the initial grid is performed by means of the so-called k-refinement. As described in [12], k-refinement procedure to enrich the *NURBS* space modifies the location of the control points in order to preserve the geometrical and parametrical representation of the surface after oder elevation and knot insertion. The definition of a projection operator that maps the control points from the enriched space back to the initial one is not trivial. For this reason, in the *IGA*-based *MGDA* procedure both the original and the refined geometry are exported from the linear elasticity solver.
Thus the global shape optimization procedure is modified to properly deal with spaces of design points of different dimensions (Step 1): the numerical simulations are executed using a set of control variables in the refined space and the analytical gradients in the higher-dimensional space are exported to run the optimization routine. Eventually the geometrical information on the evolution of the computational domain has to be correctly updated to account for the displacement of the design point towards a Pareto-stationary configuration.

Listing 4: Shape optimization procedure using *MGDA* with *NURBS*-based analytical gradients

```
1. Generate the initial geometry:
 (a) Construct the coarse grid;
 (b) If the routine is running within the optimization loop, import the updated
     position of the control points; otherwise, perform k-refinement;
2. Export the information about the geometry from both the coarse and the
   refined space;
3. Run the IGA solver:
 (a) Compute the compliance and the volume;
 (b) Extract the gradients from NURBS parametrization and export them;
4. Identify the descent direction −ω as convex combination of ∇J(Y) and ∇G(Y);
5. Determine the optimal step size ρ̃ by means of a bisection algorithm;
6. Update the design vector Y to Y − ρ̃ω;
7. If ‖ω‖ ≥ tol, go to step 1; otherwise, a Pareto-stationary design point has been
   achieved and the optimization procedure is stopped.
```

As the algorithm in script 1, this variant of *MGDA* applies to single design points thus a complete description of the first Pareto front requires several runs of the optimization procedure. Main drawback of this strategy is the resulting higher dimension of the optimization problem that causes the computational cost to increase. Nevertheless, in this framework the *IGA* solver is invoked only once per run because the objective functionals have to be evaluated only in the current configuration whereas the extraction of the components of the gradients is straightforward using the *NURBS* parametrization of the *IGA* solver. Hence, the resulting computational effort required by the *IGA*-based *MGDA* strategy is comparable with standard *MGDA* presented in section 5.1.3.

6 Numerical results

We present the test case of a two-dimensional squared flat plate with a hole located at its center and subject to uniform external normal forces. The goal is to determine the shape of the internal boundary in order to minimize the compliance for a constant plate area.

Thanks to the symmetry of the domain, we can restrict ourselves to just a quarter of the original plate. We define the computational domain by means of a single bi-quadratic patch which exhibits a singular point at the top-left corner. For the *NURBS* representation we choose quadratic basis functions, thus the singularity is obtained by introducing a control point of multiplicity two. Additional geometrical constraints are introduced to force the extremities of the moving boundary to stay on the symmetry axes.
The linear elasticity problem is approximated by means of a 12×7 net of control points; the design points of the optimization problem are represented by the control points that define the *NURBS* parametrization of the boundary Γ. Table 2 summarizes the number of optimization variables depending on the selected *MGDA* variant.
To prevent the optimization algorithm to investigate non-physical solution some precautions are necessary: the first and last point on Γ can only slide respectively horizontally and vertically and a slight penalization is imposed to keep the design points inside the domain, that is, the values of the functionals tend to worsen when the points excessively approach the symmetry lines.

6.1 Description of the first Pareto front using MGDA variants

We consider a design point in $\mathbb{R}^6$ that accounts for the coordinates of the control points of the boundary Γ as described in table 2.

First, we verify that for every admissible initial design point, *MGDA* evolution guarantees that all the criteria improve at the same time.
In figure 5a we present the convergence of *MGDA* iterates starting from several feasible initializations and we observe that both the compliance and the volume decrease at each iteration until some final Pareto-stationary points are achieved.
Figure 5b describes the corresponding evolution of the minimal-norm element $\boldsymbol{\omega}$ starting from different initial design points. In each scenario the minimal-norm element decreases at each iteration and eventually its value fulfills a sufficiently small *a priori* fixed tolerance.
This respects the scenario from the theory since we can identify a descent direction common to all the criteria until the algorithm converges towards a Pareto-stationary design point.

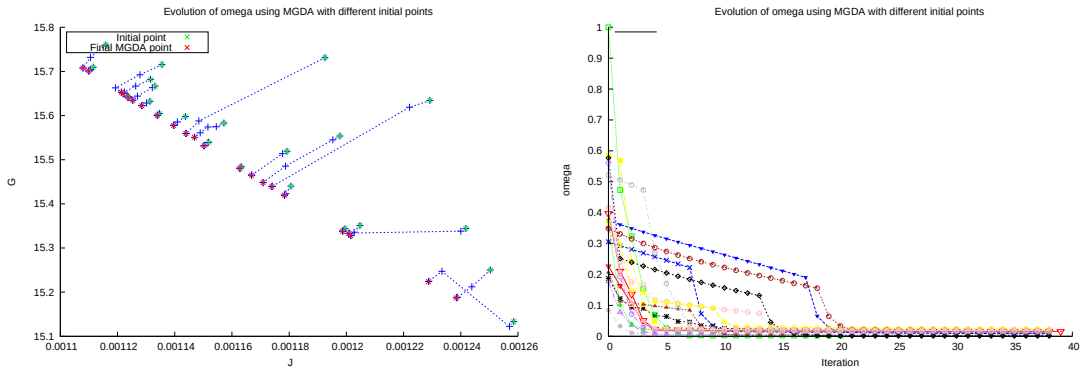

(a) Functional values in the space $J - G$.

(b) Minimal-norm element.

Figure 5: Evolution with respect to *MGDA* iterations.

Algorithm	Applies to	# Variables	# Executions	# Solver runs	CPU time [1]
MGDA using FD	30 single design points	6 (2 moving points 1 horizontally sliding 1 vertically sliding)	40 *MGDA* runs per design point	13 *IGA* runs per *MGDA* iteration	8 hours per design point
Kriging-assisted *MGDA*	Data set of 20 design points	6 (2 moving points 1 horizontally sliding 1 vertically sliding)	10 kriging-assisted runs each of which performs 60 *MGDA* iterations	1 *IGA* run per *MGDA* final point	15 hours per data set
MGDA using analytical gradients	30 single design points	34 (16 moving points 1 horizontally sliding 1 vertically sliding)	40 *MGDA* runs per design point	1 *IGA* run per *MGDA* iteration	6 hours per design point

Table 2: Computational cost of multiobjective gradient-based strategies for shape optimization using *IsoGeometric Analysis*.

Within the framework of multiobjective optimization, we seek a complete characterization of the set of Pareto-optimal solutions which requires 20 to 30 points for the problem under analysis. We present the first Pareto fronts arising from the variants of *MGDA* previously discussed and we

[1] Using dual-core CPU Intel®Core ™ 2 Duo @ 3.00 GHz and 2 GB RAM

cross-validate their reliability by means of the so-called *Pareto Archived Evolutionary Strategy*, a widely known genetic algorithm for multiobjective optimization problems.
In figure 6, we present the complete description of the first Pareto front produced by *Pareto Archived Evolutionary Strategy* and we compare it with the result of the computation performed using *MGDA* with numerical approximated gradients, kriging-assisted *MGDA* and *MGDA* using analytical gradients. The results in figure 6 confirm the consistency of the methods under analysis and provide a description of the first Pareto front which is similar in all the scenarios.
As a matter of fact, *PAES* provides a wider and more complete description of the front than

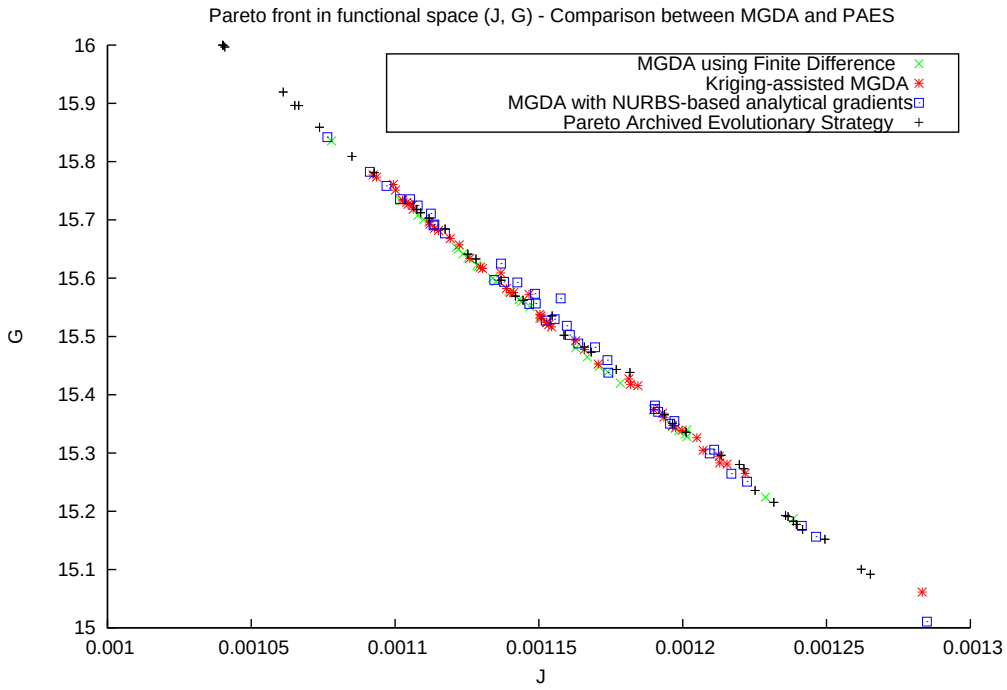

Figure 6: Comparison of the resulting first Pareto fronts in the space $J - G$.

the gradient-based approaches. Genetic algorithms are usually able to detect almost the totality of the Pareto-optimal solutions even in presence of multimodal functionals. Nevertheless, it is well known from the literature [13] that the number of configurations to be evaluated is extremely large and this results in very high computational costs. Concerning multiobjective gradient-based methods, a good approximation of the Pareto front is achieved and the overall performances strongly improve with respect to *Pareto Archived Evolutionary Strategy*. On the other hand, the discussed procedures may present some issues when dealing with multimodal functionals or initial design points not uniformly distributed over the domain.

By comparing the presented variants of the algorithm, we observe that kriging-assisted *MGDA* is responsible for a significant reduction in computing efforts: on the one hand, the *IGA* solver has to be invoked only when *MGDA* iterates already converged; on the other hand, this strategy applies to a set of design points thus is able to provide a complete description of the Pareto front after 10 to 15 runs of the algorithm. In particular, for the problem under analysis the computing time for the kriging-assisted procedure to identify a 30 points Pareto front is comparable with the one required for the evolution of two single points using standard *MGDA*.
A major drawback due to the coupling with a statistical model is the additional error introduced

in the optimization process. The first effect may be identified in the reduced extension of the the resulting Pareto front with respect to the one generated by the standard version of the algorithm: it seems that kriging-assisted *MGDA* tends to underestimate the importance of tail elements of the Pareto front and further investigation should be carried on the tuning of the parameters of the model to account for builtin sensitivities.

The results of *MGDA* variant using analytical gradients provide a validation of the strategy used to numerically approximate the gradients of the functionals by means of a second order centered Finite Difference scheme. A similar description of the first Pareto front and competitive computing times confirm the validity of standard *MGDA* for the treatment of multiobjective optimization problems.
We remark that the extraction of the analytical gradients from the *IGA* solver does not lead to a significant improvement of the performances of the algorithm: even if the number of runs of the *IGA* solver for a single iteration of *MGDA* is impressively reduced (see table 2), the optimization loop has to be performed in a higher-dimensional space and the additional control points cause the overall computing time to increase. Hence the final procedures are comparable with respect to the CPU time required for the execution.
Eventually, a summary of the complexity of the multiobjective gradient-based strategies presented in this work and their computational costs is reported in table 2.

6.2 Optimal shapes arising from MGDA variants

For the test case under analysis, the optimal shape of the hole is analytically known to be an arc of circumference (Fig. 7a). In [2] the authors verified the consistency and the reliability of a *Steepest-Descent Method* based on shape derivatives (Fig. 7b).

We use this result to compare the configurations obtained using the variants of *MGDA* pre-

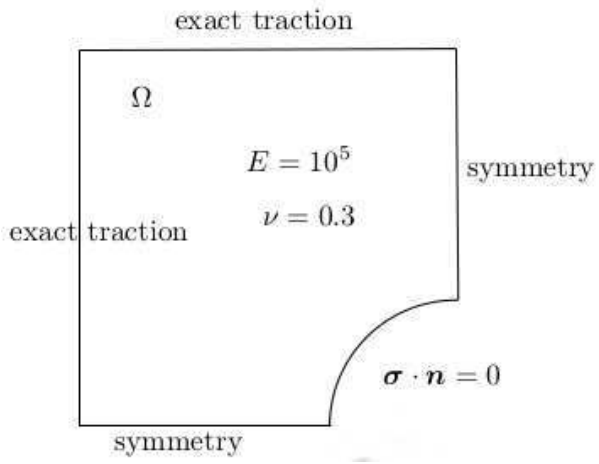

(a) Analytical optimal shape.

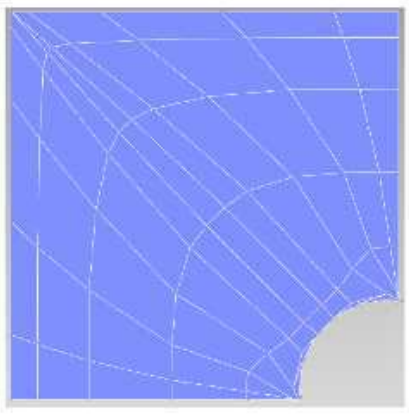

(b) Approximated optimal shape using *Steepest Descent Method* with shape derivative.

Figure 7: Comparison between the analytical and the final approximated shape.

viously introduced and we verify that the Pareto-optimal design points generate shapes which are perturbations of the analytical optimal one. This is reasonable since we aim at minimizing both the compliance and the volume of the structure at the same time. Within the framework of

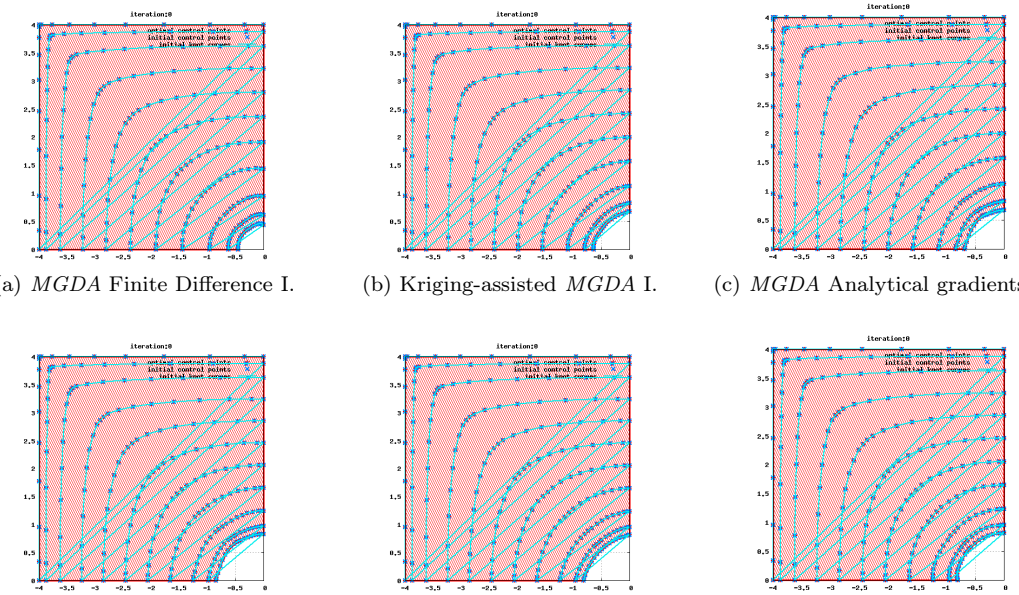

(a) *MGDA* Finite Difference I. (b) Kriging-assisted *MGDA* I. (c) *MGDA* Analytical gradients I.

(d) *MGDA* Finite Difference II. (e) Kriging-assisted *MGDA* II. (f) *MGDA* Analytical gradients II.

Figure 8: Final configurations generated by *MGDA*. Optimal shapes from the top part (first line) and bottom part (second line) of the Pareto front.

multiobjective optimization, a global optimal solution does not exist and we seek configurations that represent a trade-off between two antagonistic criteria.

In figure 8 we present two final configurations for each described algorithm. The shape of the free boundary Γ is always physically consistent with the imposed external traction and can be interpreted as perturbation of the arc of circumference in figure 7a.
Most of the differences among the final configurations are due to the choice of fostering a better optimization for one criterion rather than the other. In particular, in the first line the shapes correspond to design points where the minimization of the compliance is fostered and consequently the domain is larger. On the contrary, the second set describes the case where the minimization of the volume is fostered thus we expect the compliance to assume larger values.

7 Conclusion

We formulated a shape optimization problem within a multiobjective optimization framework and we numerically solved it using gradient-based strategies arising from the so-called *Multiple-Gradient Descent Algorithm*: both standard and kriging-assisted *MGDA* provided good results in the identification of the first Pareto front for a test case in computational mechanics. The linear elasticity problem was approximated by means of *IsoGeometric Analysis*. *NURBS*-based formulation allowed us to obtain a higher regularity on the description of the domain and on the approximation of the solution using the same parametrization for both representing the geometry and discretizing the differential problem.
On the one hand, we verified the consistency of the optimal shapes from *MGDA* simulations with the ones given by a single objective *Steepest Descent Method* based on shape derivative. On

the other one, the Pareto fronts arising from multiobjective gradient-based methods were cross-validated by using *Pareto Archived Evolutionary Strategy*. Moreover, thanks to the isogeometric paradigm, we extracted the analytical expressions of the gradients in the parametric space and we confirmed the reliability of *MGDA* procedures based on their approximation by means of Finite Difference schemes.

Possible developments of this work focus on both the formulation of a Nash game for the competitive optimization starting from a Pareto-optimal design point and the implementation of novel optimization algorithms such as cokriging-assisted *MGDA* and hybrid strategies that combine gradient-based approaches with genetic algorithms.

References

[1] G. Allaire, *Conception optimale de structures*, Springer (2006).

[2] L. Blanchard, R. Duvigneau, A.-V. Vuong, and B. Simeon, *Shape Gradient Computation in IsoGeometric Analysis for Linear Elasticity*, INRIA Research Report RR-8111 (2012).

[3] J. Cea, *Conception optimale ou identification de formes, calcul rapide de la dérivée directionnelle de la fonction coût*, ESAIM: Math. Model. Num., 20(3):371-402 (1986).

[4] A. Chambolle, *A density result in two-dimensional linearized elasticity and applications*, Arch. Ration. Mech. An., 167(3):211-233 (2003).

[5] F. de Gournay, G. Allaire, and F. Jouve, *Shape and topology optimization of the robust compliance via the level set method*, ESAIM: Contr. Optim. Ca., 14:43-70 (2008).

[6] R. Duvigneau and P. Chandrashekar, *Kriging-based optimization applied to flow control*, Int. J. Numer. Meth. Fl., 69(11):1701-1714 (2012).

[7] J.-A. Désidéri, *Cooperation and competition in multidisciplinary optimization - Application to the aero-structural aircraft wing shape optimization*, Comput. Optim. Appl., 52(1):29-68 (2012).

[8] J.-A. Désidéri, *Multiple-Gradient Descent Algorithm (MGDA) for multiobjective optimization*, C. R. Math., 350(5-6):313-318 (2012).

[9] M.C. Delfour and J.-P. Zolésio, *Shapes and geometries: analysis, differential calculus, and optimization*, SIAM, Philadelphia, USA (2001).

[10] J. Haslinger and R.A.E. Mäkinen, *Introduction to Shape Optimization: Theory, Approximation, and Computation*, SIAM, Philadelphia, USA (2003).

[11] C.O. Horgan, *Korn's inequalities and their applications in continuum mechanics*, SIAM Rev., 37(4):491-511 (1995).

[12] T.J.R. Hughes, J.A. Cottrell, and Y. Bazilevs, *IsoGeometric Analysis: CAD, finite elements, nurbs, exact geometry and mesh refinement*, Comput. Method Appl. M., 194(39-41):4135-4195 (2005).

[13] J.D. Knowles and D.W. Corne, *Approximating the nondominated front using the Pareto Archived Evolution Strategy*, Evol. Comput., 8(2):149-172 (2000).

[14] K. Miettinen, *Nonlinear Multiobjective Optimization*, Kluwer Academic Publishers Dordrecht, Netherlands (1999).

[15] F. Murat and J. Simon, *Sur le contrôle par un domaine géométrique*, Research Report 76 015, Laboratoire d'Analyse Numérique de l'Université Paris 6 (1976).

[16] L. Piegl and W. Tiller, *The NURBS book*, Springer-Verlag New York, USA (1997).

[17] O. Pironneau, *Optimal Shape Design for Elliptic Systems*, in System Modeling and Optimization - Lecture Notes in Control and Information Sciences, Vol. 38:42-66 Springer Berlin Heidelberg (1982).

[18] G. Rozza, T. Lassila, and A. Manzoni, *Reduced basis approximation for shape optimization in thermal flows with a parametrized polynomial geometric map*, Proceedings of ICOSAHOM 09, International Conference on Spectral and High Order Methods, 76:307-315 (2010).

[19] W.A. Wall, M.A. Frenzel, and C. Cyron, *Isogeometric structural shape optimization*, Comput. Method Appl. M., 197(33-40):2976-2988 (2008).

[20] A. Zerbinati, J.-A. Désidéri, and R. Duvigneau, *Application of Metamodel-Assisted Multiple-Gradient Descent Algorithm (MGDA) to Air-Cooling Duct Shape Optimization*, Proceedings in ECCOMAS 2012, European Congress on Computational Methods in Applied Sciences and Engineering, Wien, Austria (2012).

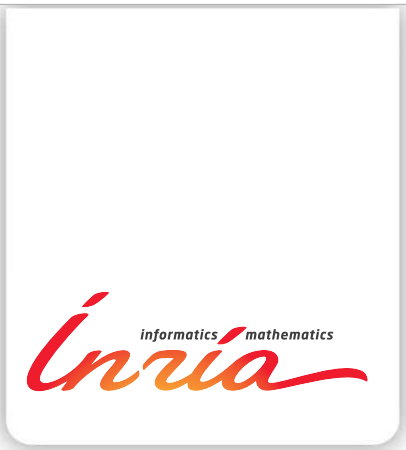

RESEARCH CENTRE
SOPHIA ANTIPOLIS – MÉDITERRANÉE

2004 route des Lucioles - BP 93
06902 Sophia Antipolis Cedex

Publisher
Inria
Domaine de Voluceau - Rocquencourt
BP 105 - 78153 Le Chesnay Cedex
inria.fr

ISSN 0249-6399